XCT DIAGNOSTIC EVALUATION OF BALLISTIC IMPACT DAMAGE IN CONFINED CERAMIC TARGETS

J.M. Wells[1], N.L. Rupert[2], W. J. Bruchey[3] and D.A. Shockey[4]

[1] *JMW Associates, 102 Pine Hill Blvd., Mashpee, MA 02649-2869, USA, jmwconsultant@comcast.net*
[2]*KLNG Enterprises, 122 Braddish Road, Kittanning, PA 16201-4306, USA, email: nevinlr@comcast.net*
[3] *Service Engineering Corp., c/o U.S. Army Research Lab., AMSRD-ARL-SL-BE, APG, MD 21005-5066, e-mail: wbruch@hughes.net*
[4] *SRI International, 333 Ravenswood Avenue, Menlo Park, CA 94025, email: donald.shockey@sri.com*

Extensive physical damage occurs upon high velocity impact in terminal ballistic ceramic targets. The characterization of this impact damage is essential to aid in the understanding of both the damage and penetration processes and of potential mechanisms for mitigating their severity. In previous studies, Shockey et al. made insightful observations of ballistic impact effects primarily based upon fractography and destructive metallographic techniques to deduce the penetration mechanism(s) for a long rod penetrator into steel encased alumina (Al_2O_3), boron carbide (B_4C), and titanium diboride (TiB_2) cylindrical ceramic targets. Recently, the authors initiated a follow up look at some of the original ceramic targets with non-invasive x-ray computed tomography, XCT, impact damage diagnostic evaluation techniques developed subsequent to the original Shockey et al. study. Meso-scale impact damage manifestations in these ceramic target samples include irregularly shaped discontinuous embedded projectile fragments, inhomogeneous impact-induced porosity, and extensive surface and interior cracking. Initial qualitative and quantitative results are reported and discussed along with segmented 3D virtual images to further assist in the cognitive visualization of the damaged conditions.

INTRODUCTION

The goal of the original work reported by Shockey et al [1-3] was to establish the failure phenomenology of steel encased and confined ceramic targets and tungsten-nickel-iron alloy impacting long rods during penetration, and to deduce the ceramic properties governing penetration resistance. The failure mechanisms and properties controlling penetration behavior were inferred from fractographic and metallographic examination of the targets and rods after impact. Subsequent to that original study, x-ray computed tomography, XCT, diagnostic techniques for impact damage characterization and visualization were independently developed and demonstrated [4-6] in separate ballistic impact damage studies of various armor ceramic targets. With the relatively

recent introduction of quantitative and volumetric impact damage diagnostics using XCT, significant inroads have been made in expanding our knowledge base of the morphological variants of physical impact damage. To date, there is surprising little actual impact damage characterization data available in detail, especially on a 3D volumetric basis. Thus, the authors decided to apply such XCT diagnostic techniques to augment findings on three of the identical samples from the original Shockey et al. study.

In this initial brief report on the recent volumetric XCT diagnostic results, we are focusing on the damage features of residual projectile fragments and impact-induced porosity, both details which are commonly unreported in most terminal ballistic studies. Obviously, the various modes of impact-induced cracking and the fragmentation of the ceramic are very important as well and will be dealt with in a subsequent publication.

XCT IMPACT DAMAGE DIAGNOSTIC TECHNIQUES

XCT is an enabling 3D nondestructive diagnostic modality which permits the virtual interrogation of impact damage features both on the surface and within the bulk of the ballistic target. It uses the triangulation of volumetric x-ray absorption data to construct a completely digitized "density" map of a solid object thus accurately representing the dimensional and structural features of that object. Achievable resolution levels with the XCT modality depend upon the object size, density, and the x-ray source and detector system. The nominal resolution level for the meso-scale tomography of a modest size (~$3x10^6$ mm^3) medium density laboratory ballistic target is <0.250 mm. Micro-tomography resolution levels of < 20 microns are achievable but on relatively less dense and/or smaller objects of ~10^4 mm^3. If considerably higher resolution levels are still required then destructive sectioning and high resolution electron microscopy techniques may augment the results of XCT.

Once the physical target has been digitized by XCT scanning, all subsequent interrogations of that impacted target are conducted in the *virtual* diagnostic domain. The original XCT scan data file of each target is reconstructed into a virtual 3D solid object using a commercially available voxel analysis and visualization software package [7]. A variety of image processing tools and routines are then used to create the virtual XCT diagnostic images which contribute to the enhanced understanding of various physical impact damage details. Such a noninvasive approach generally can augment, and even avoid the limitations of, destructive sectioning, polishing, etching and metallography. The XCT diagnostic results are reproducible, accessible, and amenable to digital archival file storage. XCT ballistic impact diagnostic capabilities typically include: external radial and circular surface cracking and topological irregularities, subsurface (internal) impact damage cracking morphological features, orthogonal (axial, frontal, and sagittal) virtually sectioned views as well as arbitrary angle virtual planar sectioning, inhomogeneous impact-induced porosity characterizations (e.g. pore size,

spatial location, and volumetric distribution), residual projectile fragment characterization (e.g. spatial position, size, morphology, surface area and volume), in-situ metrology including linear, area, volume, angle dimensions, gray level differentiation, and 3D visualizations of all such damage features.

IMPACTED CERAMIC TARGETS

Details of the original rod impact experiments and resulting damage observations are given in the prior papers by Shockey et al. [1-3]. Three sections (half-cylinders) of the original impacted samples examined in the current work are shown in figure 1. Measurements of their respective macroscopic dimensions are presented in Table 1.

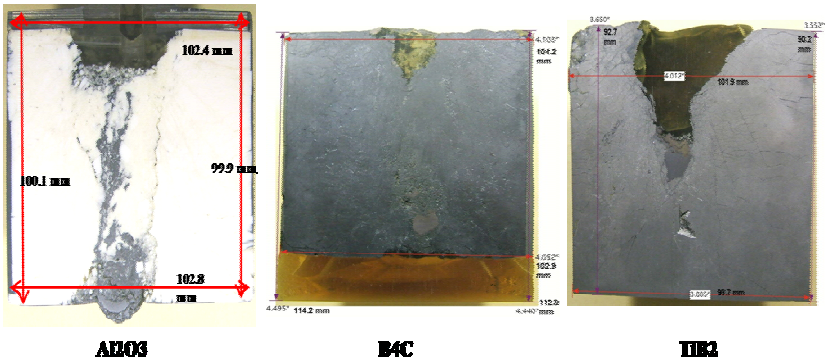

Figure 1. Macro-images of the 3 ceramic targets examined in this study (impact surface on top).

Table I. Measured Dimensions of Impacted Ceramic Target Samples

Ceramic Target	Height mm	Diameter (Width) mm	Projectile Penetration Observations
Al_2O_3	99.9 – 100.1	102.4 – 102.8	Full & Discontinuous
B_4C	112.8 – 114.2	102.9 –104.2	Full & Intermittent
TiB_2	90.2 – 92.7	98.7 – 101.9	Partial & Intermittent

EMBEDDED PROJECTILE FRAGMENTS

A reconstructed 3D solid object of the B_4C ceramic target is shown in figure 2, both as an opaque object and in a virtually transparent view revealing the morphology and distribution of internal residual projectile fragments. Here, it is observed that the projectile fragments are intermittent along the projectile path and essentially located in close radial proximity along the path of the projectile penetration. The residual fragment mass seen at the top of the figure appears largest but actually is an agglomeration of several smaller fragments identified as 7A, 8A, 9A,10A, and 11A.

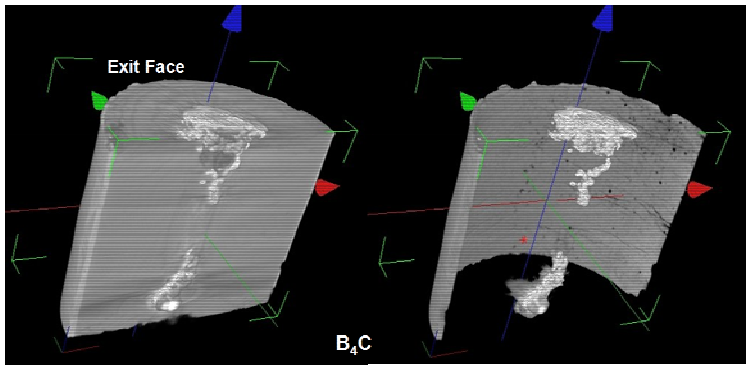

Figure 2. Two 3D solid object images of B_4C target – Opaque (left) and transparent (right)

Some quantitative diagnostic results of the more substantial individual fragments were obtained and are shown in figure 3. Eleven fragments are identified with measurements of their position, approximate size (e.g. bordering dimensions), surface area and volume. Some smaller, less substantial, fragments were not included in this quantification but may still be observed in figure 3. Such residual fragment segmentation, characterization, and visualization results are not readily available without XCT diagnostic techniques.

Projectile Fragment ID	3D Location – slice# < Sag-Frontal-Axial>	Bordering Dimensions, mm	Surface Area mm²	Volume mm³
P-F #1A	< S212 F22 A84 >	14.82 x 4.61 x 19.12	416.30	264.32
P-F #2A	< S238 F29 A181 >	3.22 x 3.65 x 6.57	28.14	6.54
P-F #3A	< S262 F33 A172 >	54.18 x 7.20 x 37.14	7.42	1.38
P-F #4A	< S247 F22 A328 >	3.85 x 3.44 x 5.89	47.53	8.22
P-F #5A	< S239 F22 A342 >	1.50 x 0.86 x 1.29	4.17	0.68
P-F #6A	< S271 F22 A393 >	1.07 x 0.84 x 1.72	2.73	0.32
P-F #7A	< S268 F22 A440 >	4.94 x 5.69 x 9.02	119.41	20.47
P-F #8A	< S283 F22 A446 >	2.15 x 1.72 x 1.93	7.52	1.13
P-F #9A	< S191 F22 A444 >	2.36 x 1.93 x 1.50	9.13	1.27
P-F #10A	< S265 F33 A449 >	3.01 x 1.50 x 3.01	14.38	2.57
P-F #11A	< S279 F26 A450 >	2.15 x 1.72 x 1.93	7.35	1.08

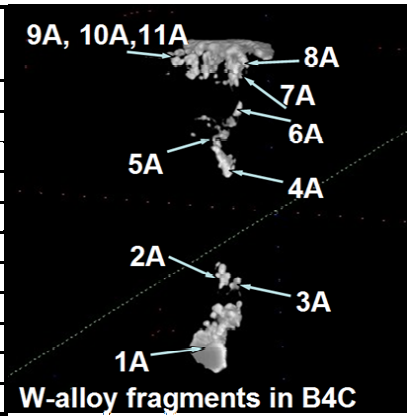

Figure 3. Characterization data (left) and transparent (right) visualization of residual projectile fragments are shown for the B_4C ceramic target.

In the case of the TiB_2 ceramic target examined, partial penetration was observed with intermittent projectile fragments observed only in the upper portion of the target. Two large separated and irregular shaped fragments are observed in figure 4, with more multiple smaller fragments becoming visible in the host TiB_2 ceramic with the fully virtual transparent mode. A large horizontally oriented dark band is also seen in the fully opaque reconstructed image on the left and is considered an artifact indicative of a reduced fluence of x-ray photons received at the linear detector array at

the scan height coincident with the large higher density mass of the embedded fragment. Contrary to their initial appearance, the two large fragment masses have a complex sub-structure consisting of small high density projectile fragments agglomerated with a mixture of fine debris from both the projectile and the host ceramic. Details of this substructure are shown for the upper fragment mass in figure 5.

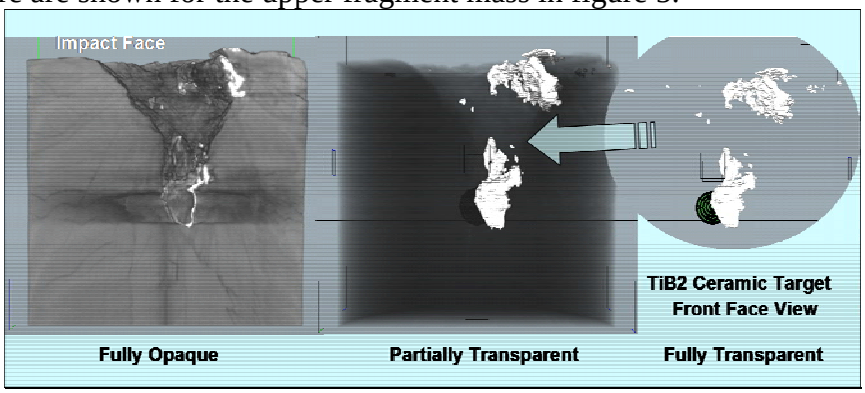

Figure 4. Variable transparency technique revealing w-alloy projectile fragments within the TiB_2 ceramic.

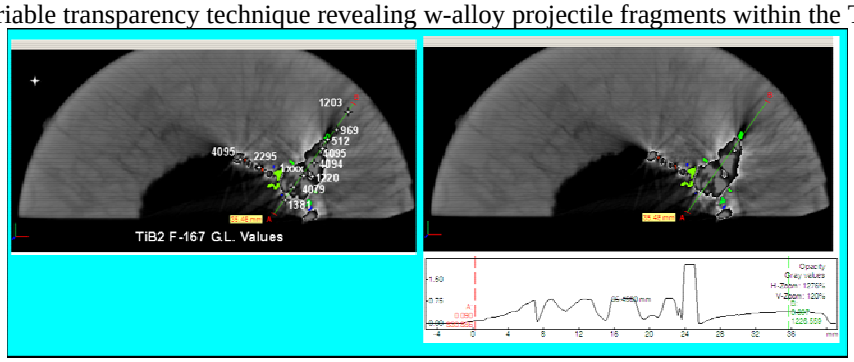

Figure 5. Grey level measurements observed on XCT axial slice A-167 indicate sub-structure with significant density variations in the upper fragment mass in the TiB_2 ceramic target.

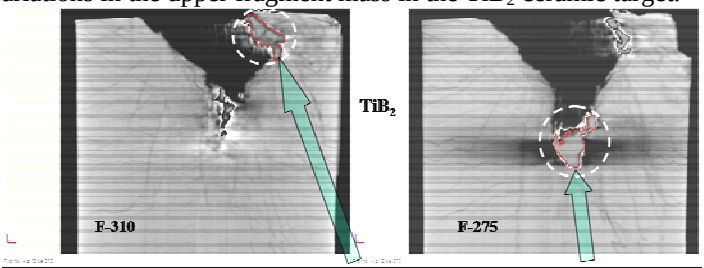

	Upper Fragment	Lower Fragment
Mean Grey Level	3256	3505
GL Deviation	692.4	613.4
Surface Area, mm²	1,512.45	1012.25
Volume, mm³	1215.78	980.72
Enveloping Dimensions, mm	18.25 x 25.75 x 16.50	12.75 x 12.75 x 30.50

Figure 6. Segmentation characterization values for upper & lower projectile fragments in TiB2.

Metrology data for the two largest embedded projectile fragments are show in figure 6. The lower residual fragment is actually ~ 24 % smaller in volume than the upper fragment, although it appears larger in the frontal slice F-275.

A similarly rendered 3D solid object reconstruction of the Al_2O_3 ceramic target is shown in figure 7. The residual projectile w-alloy fragments embedded in this ceramic is observed to be discontinuous and essentially aligned through the target thickness with varying cross-sections, with the largest fragment cross-section located near the bottom exit face. Expanded views of the fragment cross sections reveal considerable sub-structural complexity of the fragment masses on the five virtual sections indicated.

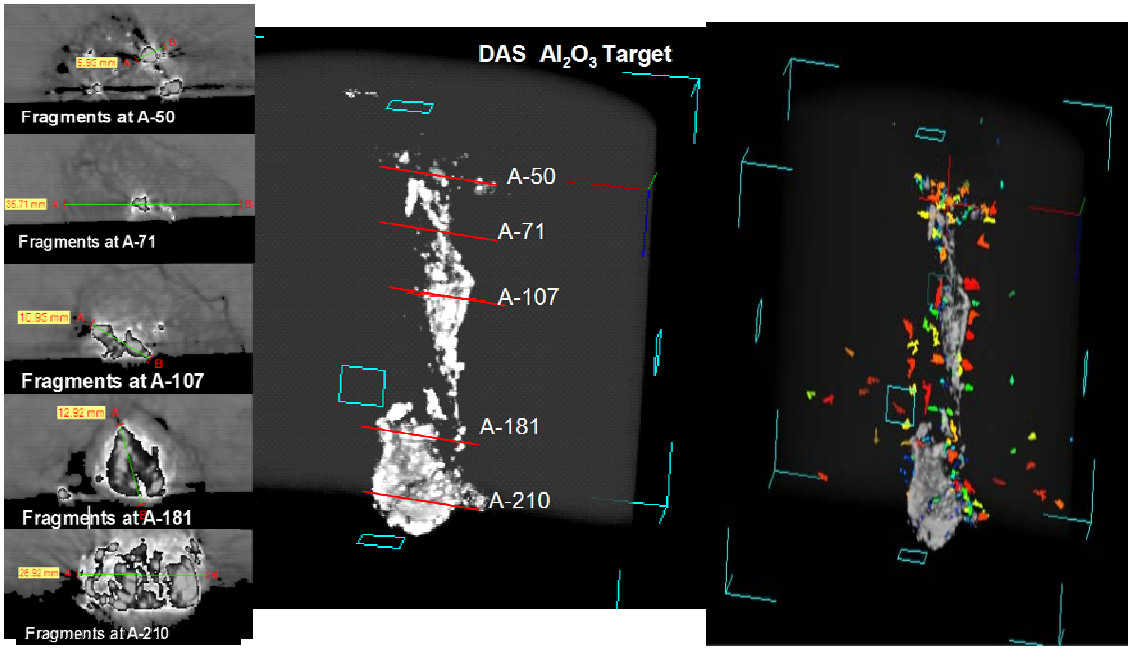

Figure 7. A 3D solid object semi-transparent image (center) with close up views of fragment cross sections at five virtual axial sections as indicated (left) and impact-induced porosity (right).

Interestingly, multiple *low* density "orbital" voids are observed and shown completely through the target thickness adjacent to the longitudinal fragments in the transparent orthogonal view. The voids appear located at radii beyond the extremities of the longitudinal fragment in a pattern roughly replicating the irregular profile of that fragment.

IMPACT-INDUCED POROSITY

While many different and quite varied impact damage defects of other types have been observed resulting from terminal ballistic testing of armor ceramics [4-6], relatively

little attention has been focused on *impact-induced* porosity and its potential effect(s) on overall ballistic performance. Practical methods for non-invasively studying and evaluating impact-induced porosity are quite limited since traditional NDE modalities have significant limitations in their technical capabilities to spatially locate, characterize, quantify, and visualize such internal porosity. The XCT techniques have been demonstrated [8] to be quite effective in the characterization, visualization, and analysis of volumetric porosity in engineering castings. For the ballistic situation, the observation of an impact-induced mesoscale porosity level of ~1.94% in a separate TiB_2 armor ceramic target was reported earlier [9]. The current work reveals the presence of impact-induced porosity in all three ceramic targets. Significant differences in porosity amounts, size and inhomogeneous spatial distribution are apparent. The porosity results presented have been segmented from the other multiple impact-induced damage manifestations by virtual transparency and pseudo-color variations for improved cognitive visualization.

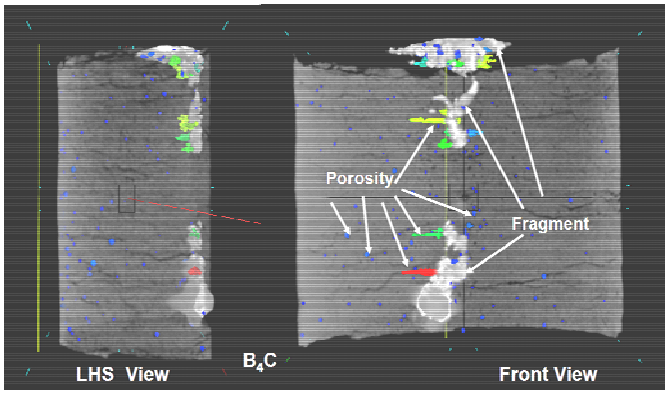

Figure 8. Observations of impact-induced porosity are revealed in virtually transparent left hand side and frontal views of B_4C ceramic target. Small pores are primarily in outer epoxy coating, while larger hi aspect ratio porosity is located within host B4C ceramic adjacent to embedded discontinuous projectile fragments.

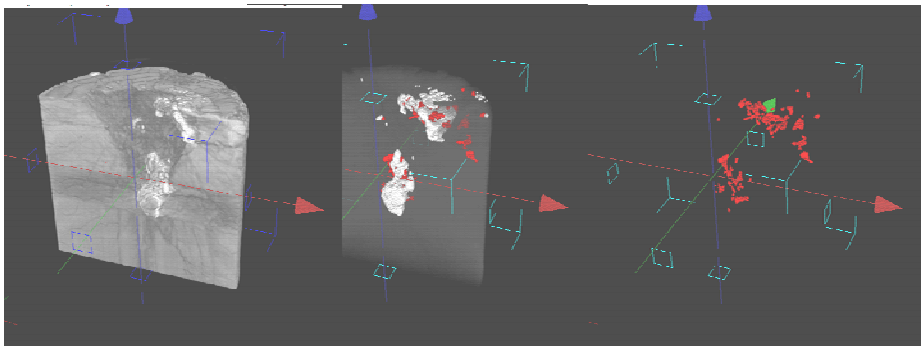

Figure 9. Observations of impact-induced porosity are shown in red within TiB_2 ceramic semi-transparent and fully transparent virtual images.

SUMMARY

The functionality and capabilities of the non-invasive XCT diagnostic characterization of residual projectile fragments is demonstrated for partial and full penetration terminal ballistic ceramic targets. Density (gray level) and morphological segmentation and virtual transparency reveal the distribution, spatial position, relative size, shape, and inner complexity of embedded projectile fragments. Virtual metrology permits the measurement of the fragment linear, surface area, and volume dimensions. 3D virtual images of these features greatly assist in their cognitive visualization.

The traditional concern with porosity in technical ceramics utilized for protective armor applications has been focused on reducing inadvertent defects introduced during their manufacturing processing to very low levels (<1%) of micro-porosity. The impact-induced mesoscale porosity features demonstrated here are substantially greater in pore size and volume, and tend to be asymmetrically localized in the vicinity of substantial sized embedded projectile fragments. The relative contribution of such inhomogeneous impact-induced porosity affecting the total ballistic penetration process remains to be studied and characterized. Further work is also required to achieve an XCT statistical size and distribution analysis of the host ceramic fragmentation.

ACKNOWLEDGEMENTS

Grateful acknowledgements are extended to Mr. William Green of ARL for conducting the XCT digital scans and to Dr. Christof Reinhart for assistance with the Volume Graphics StudioMax software.

REFERENCES:

[1] D.A. Shockey, A.H. Marchand, S.R. Skaggs, G.E. Cort, M.W. Burkett and R. Parker, "Failure Phenomenology of Confined Ceramic Targets and Impacting Rods," *International Journal of Impact Engineering*, v 9 (3), 263-275, (1990)
[2] D.A. Shockey, D.R. Curran, R.W. Klopp, L. Seaman, C.H. Kanazawa, and J.T. McGinn, "Characterizing and Modeling Penetration of Ceramic Armor," ARO Report No. 30488-3-MS, (1995)
[3] D.A. Shockey, A.H. Marchand, S.R. Skaggs, G.E. Cort, M.W. Burkett and R. Parker, "Failure Phenomenology of Confined Ceramic Targets and Impacting Rods," Ceramic Armor Materials by Design, Ed. J.W. McCauley et. al., Ceramic Transactions, v134, ACERS, 385-402 (2002)
[4] J.M. Wells, N. L. Rupert, and W. H. Green, "Progress in the 3-D Visualization of Interior Ballistic Damage in Armor Ceramics," Ceramic Armor Materials by Design, Ed. J.W. McCauley et. al., Ceramic Transactions, v134, ACERS, 441-448 (2002)
[5] J.M. Wells, "Progress in the NDE Characterization of Impact Damage in Armor Materials," *22nd International Ballistics Symposium*, v2, 793-800 (2005)
[6] J.M. Wells, "On Incorporating XCT into Predictive Ballistic Impact Damage Modeling,"*22nd International Ballistics Symposium*, v2, 1223-1230 (2005)
[7] Volume Graphics StudioMax v1.2.1, www.volumegraphics.com
[8] J.M. Wells, "Quantitative XCT Evaluation of Porosity in an Aluminum Casting," Proc. 2nd Intn'l Symposium on Shape Casting, TMS (2007) In Press.
[9] J.M. Wells and R.M. Brannon, "Advances in XCT Diagnostics of Ballistic Impact Damage," Dynamic Behavior of Materials, ed. by N. Thadhanki et al, TMS, (2007) In Press.